AGU ADVANCING EARTH AND SPACE SCIENCE

Geophysical Research Letters

RESEARCH LETTER
10.1029/2021GL093173

Causes of Jets in the Quasi-Perpendicular Magnetosheath

Primož Kajdič[1], Savvas Raptis[2], Xóchitl Blanco-Cano[1], and Tomas Karlsson[2]

[1]Departamento de Ciencias Espaciales, Instituto de Geofísica, Universidad Nacional Autónoma de México, Ciudad Universitaria, Ciudad de México, Mexico, [2]Space and Plasma Physics, KTH Royal Institute of Technology, Stockholm, Sweden

Abstract Magnetosheath jets are currently an important topic in the field of magnetosheath physics. It is thought that 97% of the jets are produced by the shock rippling at quasi-parallel shocks. Recently, large statistical studies of magnetosheath jets have been performed, however, it is not clear whether rippling also produces jets found downstream of quasi-perpendicular shocks. We analyze four types of events in the quasi-perpendicular magnetosheath with signatures characteristic of magnetosheath jets, namely increased density and/or dynamic pressure that were not produced by the shock rippling: (a) magnetic flux tubes connected to the quasi-parallel bow-shock, (b) nonreconnecting current sheets, (c) reconnection exhausts, and (d) mirror-mode waves. The flux tubes are downstream equivalents of the upstream traveling foreshocks. Magnetosheath jets can impact the magnetopause, so knowing the conditions under which they form may enable us to understand their signatures in the magnetosphere.

Plain Language Summary Magnetosheath jets have been identified as strong local enhancements of dynamic pressure or similar quantity in the magnetosheath associated to velocity and/or density enhancements. It is currently thought that ∼97% of magnetosheath jets form due to rippling of the quasi-parallel bow-shock. However shock rippling at the quasi-perpendicular shock occurs on much smaller spatial scales (∼5 d_i, upstream ion inertial scales) than at the quasi-parallel shock (several tens of d_i). It is thus not clear whether the rippling produces magnetosheath jets at the quasi-perpendicular shock. Here, we show for the first time four different phenomena, not associated to shock rippling, that can produce magnetosheath jets in the quasi-perpendicular magnetosheath. Three of them are already known types of events: current sheets, reconnection exhausts, and mirror-mode waves. The fourth phenomena are magnetic flux tubes that are embedded in the quasi-perpendicular magnetosheath but are connected to the quasi-parallel bow-shock.

Key Points:

- Jets in the quasi-perpendicular (Qper) magnetosheath may be of different origin than those in the quasi-parallel magnetosheath
- Some causes of jets in the Qper magnetosheath are known phenomena, such as mirror-mode waves, current sheets, and reconnection exhausts
- Some jets in the Qper magnetosheath are due to passing magnetic flux tubes, which are downstream equivalents of traveling foreshocks

Correspondence to:
P. Kajdič,
primoz@igeofisica.unam.mx

Citation:
Kajdič, P., Raptis, S., Blanco-Cano, X., & Karlsson, T. (2021). Causes of jets in the quasi-perpendicular magnetosheath. *Geophysical Research Letters*, *48*, e2021GL093173. https://doi.org/10.1029/2021GL093173

Received 2 MAR 2021
Accepted 14 JUN 2021

1. Introduction

The interaction of the solar wind (SW) with our planet's magnetosphere produces a supercritical (Treumann, 2009) collisionless bow-shock upstream of Earth (e.g., Tsurutani & Stone, 1985). Depending on the angle between the local shock normal and the upstream B-field, θ_{BN}, the bow-shock can be classified as quasi-parallel (Qpar, $\theta_{BN} < 45°$) or quasi-perpendicular (Qper, $\theta_{BN} > 45°$). Upstream of Qpar shocks the foreshock is formed (Eastwood et al., 2005). Such shocks present strong rippling at the spatial scales of $\lesssim$100 upstream ion inertial lengths (d_i, e.g., Burgess, 1989; Krauss-Varban & Omidi, 1991).

Downstream of the bow-shock there lies the magnetosheath (e.g., Lucek et al., 2005) which is bounded by the magnetopause. Depending on which portion of the bow-shock the magnetosheath is magnetically connected to, we distinguish Qper and Qpar magnetosheath (Raptis, Karlsson, et al., 2020). The latter is populated by stronger B-field and plasma fluctuations and more energetic ions with energies of up to ∼30 ke V.

Magnetosheath jets are also found in the magnetosheath (Plaschke et al., 2018, and the references therein). T. V. Hietala et al. (2009) suggested that these jets form due to different processing of the SW at different locations on the Qpar bow-shock, caused by the rippling. H. Hietala and Plaschke (2013) estimated that 97% of the observed jets are produced by the bow-shock ripples. Archer et al. (2012) associated jets to IMF rotational discontinuities, while Savin et al. (2012) linked them to hot flow anomalies (e.g., Lucek et al., 2004). Karlsson et al. (2012) associated a subset of magnetosheath jets, called plasmoids, to either plasmoids from the pristine SW or short large amplitude magnetic structures (e.g., Giacalone et al., 1993) from the foreshock that are transmitted into the magnetosheath.

In the past, statistical studies with large numbers of magnetosheath jets have been performed (Archer & Horbury, 2013; Liu et al., 2020; Plaschke et al., 2013, 2016; Raptis, Aminalragia-Giamini, et al., 2020; Raptis, Karlsson, et al., 2020), however, their primary focus was not the jets' origin.

Knowing the causes of the jets is important, since it has been shown that they can perturb the geomagnetic field. Blanco-Cano et al. (2020) found jets formed by magnetic reconnection at the magnetopause. Some jets were observed to impact and sometimes penetrate the magnetopause (Dmitriev & Suvorova, 2012; H. Hietala et al., 2018; Plaschke & Glassmeier, 2011; Plaschke et al., 2016; Savin et al., 2012; Shue et al., 2009; Wang et al., 2018) and even perturb the ionosphere (Archer & Horbury, 2013; N. Hietala et al., 2012; Wang et al., 2018). They were found by Archer and Horbury (2013) to be able to drive compressional and poloidal Pc5 (2–7 mHz) waves in the magnetosphere. Finally, their signatures in the data of ground-based magnetic observatories have been reported by Dmitriev and Suvorova (2012) and Archer and Horbury (2013).

In this work, we show that certain phenomena in the Qper magnetosheath, some of them already known, may produce signatures in the spacecraft data, such as increased dynamic pressure (P_{dyn}), that would classify them as magnetosheath jets. These are magnetic flux tubes embedded in Qper magnetosheath that are connected to the Qpar bow-shock, nonreconnecting current sheets (CSs), reconnection exhausts (REs), and mirror-mode (MM) waves.

2. Instrumentation

We use data from three multi-spacecraft missions in the orbit around Earth: Cluster (Escoubet et al., 1997), THEMIS (Angelopoulos, 2008), and Magnetospheric Multiscale Mission (MMS, Sharma & Curtis, 2005). The Cluster probes carry several instruments, including a fluxgate magnetometer (FGM, Balogh et al., 2001) and the Cluster Ion Spectrometer (CIS, Rème et al., 2001). We use FGM *B*-field vectors and CIS-HIA ion moments with 0.2 and 4 s time resolution, respectively. THEMIS data used in this work were provided by the FGM (Auster et al., 2008) and ion electrostatic analyzer (McFadden et al., 2008) with 0.25 and 3 s resolution, respectively. In the case of MMS, we use *B*-field data provided by the FGM (Russell et al., 2016) with time resolution of 128 and 16 s^{-1} in the burst and survey mode, respectively. The ion data provided by the fast plasma investigation (Pollock et al., 2016) have 150 ms and 4 s time resolution in the burst mode and survey mode, respectively.

3. Observations

In this section, we show events that exhibited significantly enhanced P_{dyn} in the Qper magnetosheath. These satisfy at least some of the criteria described in the past literature, for example, we selected them if they produced P_{dyn} increases of ≥50% compared to the ambient values during a 10-min time interval, as in Gutynska et al. (2015). Additionally, two events, a passing flux tube and a CS, satisfy the criteria of Archer et al. (2012) that P_{dyn} should exceed 1 nPa. The MM waves comply with the criteria of Karlsson et al. (2012) that the density increase inside the jets should increase by 50% compared to the surrounding values.

3.1. Magnetic Flux Tubes Connected to the Qpar Bow-Shock

We first discuss what is meant by the Qpar and Qper magnetosheath. Figure 1 shows MMS1 observations during two time intervals, on March 1, 2018 (a) and on March 7, 2018 (b). The panels from (i) to (ix) exhibit: *B*-field magnitude and components in units of nT and in GSE coordinates (*X*-axis pointing from the Earth toward the Sun, the *Y*-axis lies in the ecliptic plane and is pointing toward dusk, *Z*-axis completes the right-hand system), the ion density (in cm^{-3}), parallel and perpendicular temperatures (eV), the temperature anisotropy defined as T_{per}/T_{par}, the total ion velocity and GSE components (kms^{-1}), the dynamic pressure (nPa) and the ion spectrogram with the colors representing the logarithm of the particle energy flux (PEF) in units of keV/(s cm^2 sr keV).

The crucial panels are those numbered with roman numbers (iv), (v), and (ix). In the case of the Qper (Figure 1a), magnetosheath the ion T_{per} (red) is larger than T_{par} (blue). Thus, T_{per}/T_{par} is above 1. Due to large T_{per}, the shocked SW signature in the ion spectrogram (red trace on panel ix) is very wide. Also, there are very few ions at energies above 2,500 eV. We compare these panels to those in Figure 1b which exhibit the

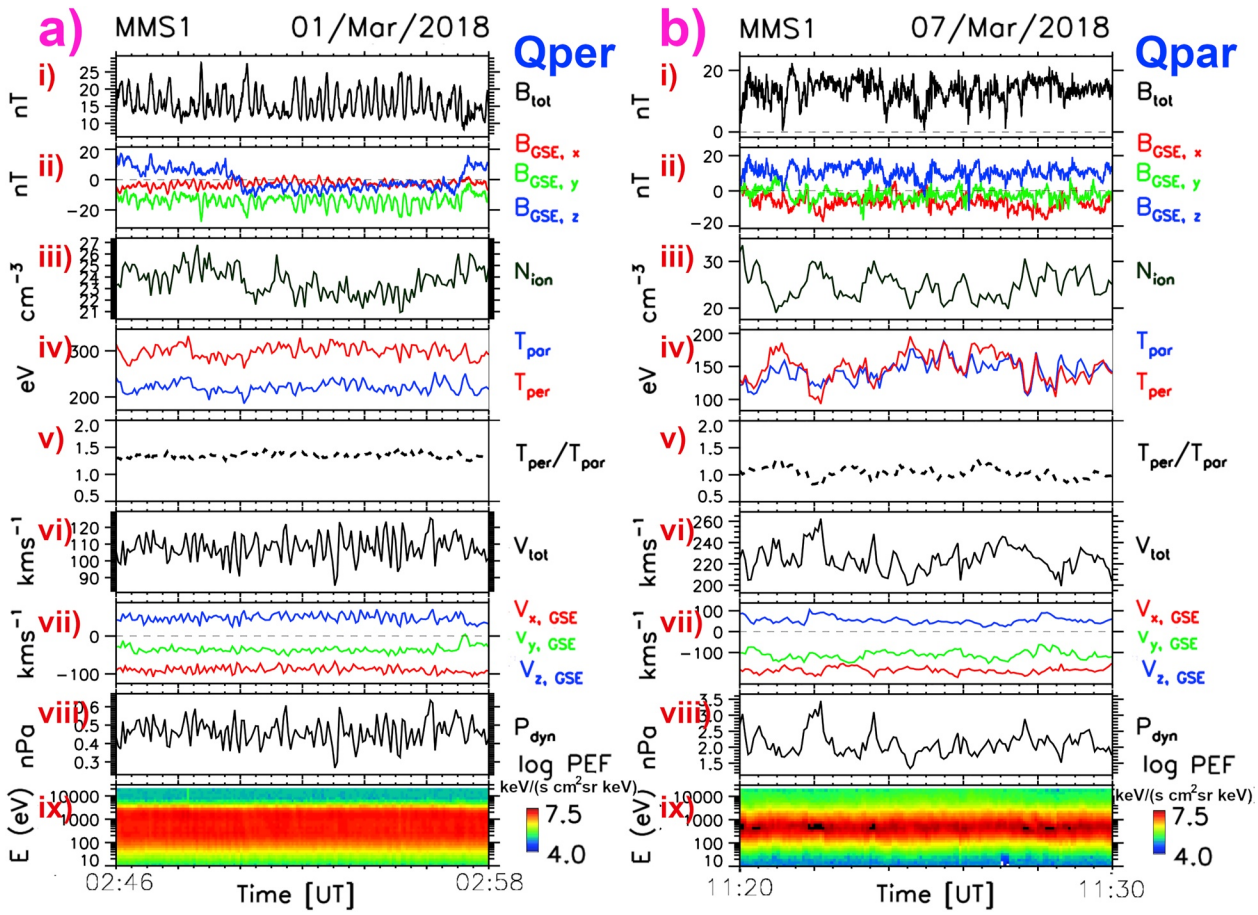

Figure 1. Magnetospheric Multiscale Mission (MMS) 1 observations of the Qper (a) and Qpar (b) magnetosheath. The panels exhibit: (i) *B*-field magnitude, (ii) *B*-field components in the GSE coordinate system, (iii) ion density, (iv) ion parallel (blue) and perpendicular (red) temperatures, (v) temperature anisotropy, (vi) total ion velocity, (vii) ion velocity components, (viii) dynamic pressure, and (ix) ion spectrogram.

Qpar magnetosheath. Now T_{par} and T_{per} exhibit very similar values resulting in T_{par}/T_{per} ~1. The values of the two temperatures are similar to the T_{par} in Figure 1a. Hence the red trace on the panel (ix) is narrower, however, the PEF intensity at energies above 2,500 eV is much higher.

We now turn our attention to Figure 2a. The format of this figure is basically the same as that of Figure 1. During most of the exhibited time interval Cluster-3 is located in the Qper magnetosheath. However, there is a short time period between 21:20:30 and 21:21:45 UT when ions with $E \lesssim 30$ keV can be observed. During this time the B_{tot}, ion density, T_{per}/T_{par} and total velocity values are diminished, while the T_{per} and T_{par} are enhanced. These signatures are very similar to those observed in the Qpar magnetosheath.

This region is bounded by rims where B_{tot}, N_{ion}, and V_{tot} are enhanced and the temperature is diminished. In the upstream rim the *B*-field rotates during ~4 s and this is also an approximate duration of this rim in the B_{tot} data. The *B*-field rotation in the downstream rim is much longer, lasting ~30 s. The high-energy ions appear and disappear during these rotations. We can also observe that the P_{dyn} in the downstream rim is strongly enhanced—it reaches 2.9 nPa, which represents a 107% increase compared to the ambient value of 1.4 nPa. It would be classified as an encapsulated jet by Raptis, Aminalragia-Giamini, et al. (2020).

This structure was convected pass the Cluster spacecraft. This can be seen in Figure 2b which shows B_{tot} profiles from all Cluster probes. C3 was the first to detect the structure, followed by C2, C4, and C1. This order is the same as the order in which their X_{GSE} coordinates decrease (Figure 2c).

This structure is different from "typical" jets found in the Qpar magnetosheath. We argue here that the signatures featured in Figure 2 are due to a magnetic flux tube that was convected pass the Cluster probes. This

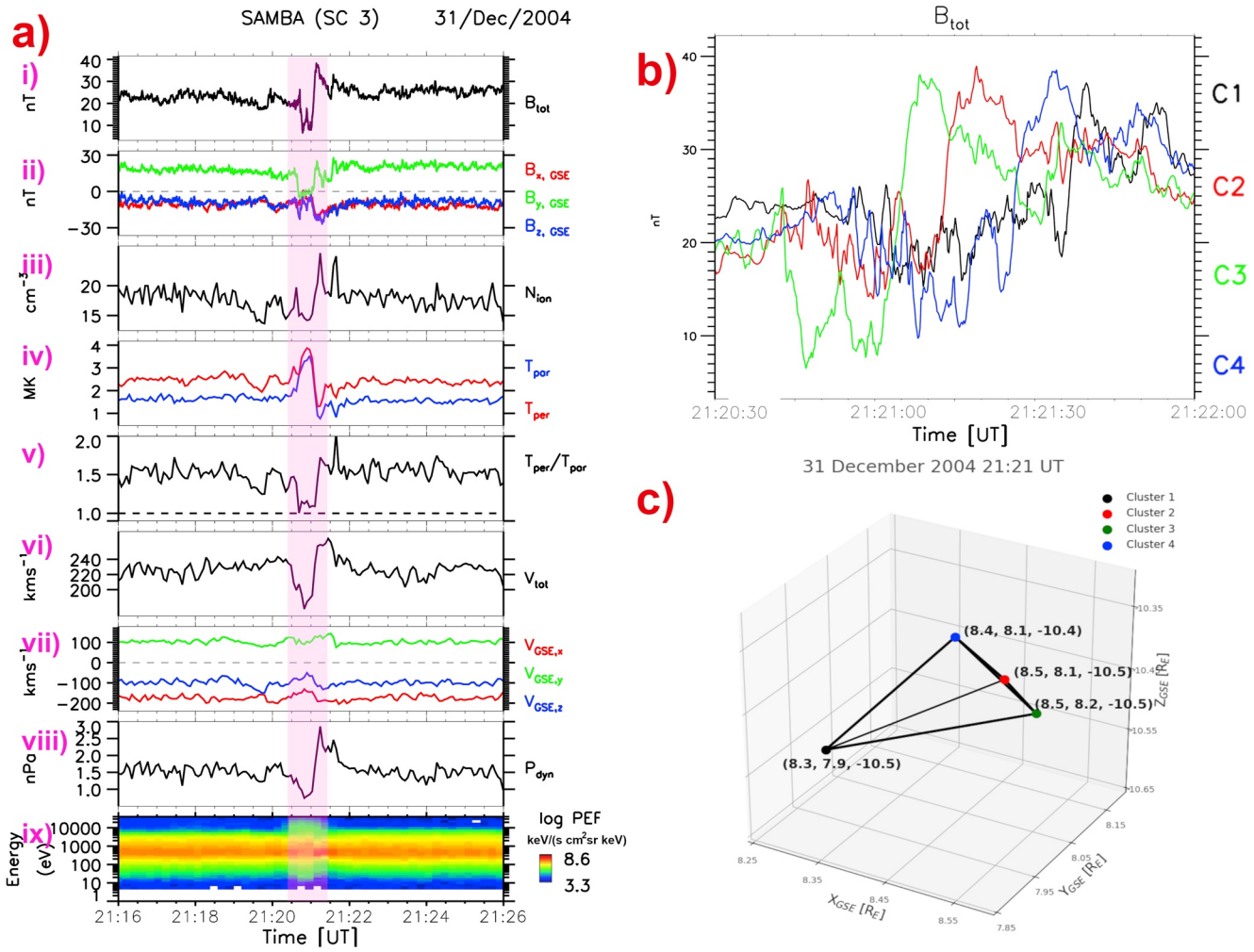

Figure 2. (a) Cluster-3 observations. The format is the same as in Figure 1a. (b) *B*-field profiles of the convected flux tube in (shaded region in a) all four Cluster spacecraft data. (c) Configuration of the Cluster constellation on December 31, 2004.

tube exhibited either small transverse radius or it was wide and was crossed by the spacecraft near its edge. Equivalent situations have been observed upstream of the Qper section of the Earth's bow-shock. Common phenomena include the foreshock cavities (e.g., Billingham et al., 2008; Sibeck et al., 2002), which are observed in pristine SW, but the IMF and plasma properties inside them are the same as those typically found in the Earth's foreshock. Compared to their surroundings, foreshock cavities exhibit depressed density and magnetic field values in their cores, while these quantities are enhanced in their rims. Also, suprathermal ion fluxes are highly enhanced inside these events. Omidi et al. (2013) and Kajdič et al. (2017) showed that foreshock cavities are a subset of traveling foreshocks with short duration in the spacecraft data. It was suggested that the traveling foreshocks form due to magnetic flux tubes that are observed upstream of the Qper bow-shock but are connected to the Qpar section of the bow-shock.

The reason we know that the observed event is caused by a magnetic flux tube and not by the back and forth motion of the boundary between the Qper/Qpar magnetosheath is because the convected flux tubes produce the so called convected signatures when they are observed by multiple spacecraft, while the back and forth boundary motion produces nested signatures (see Kajdič et al., 2017, for details). In the first case (Figure 2b), the sequence in which the spacecraft enter a passing magnetic flux tube is the same as the sequence in which they exit it. If the spacecraft had observed back and forth motion of the boundary between the Qper and Qpar magnetosheath, the Cluster probes would enter the Qpar magnetosheath in a certain sequence but the sequence in which they would exit it would be reversed. Signatures of passing flux tubes

have been reported in the past by, for example, Sibeck et al. (2000) and Katrcolu et al. (2009) who studied their impact on the magnetopause motion. Katrcolu et al. (2009) called these events the magnetosheath cavities.

In order to see what a longer lasting flux tube looks like in the data, we analyze the event in Figure 3. We can observe IMF and plasma signatures of the Qper magnetosheath before and after the event (shaded in purple), while during the event IMF and plasma exhibit properties typical of those in the Qpar magnetosheath. The duration of this event in the data is ∼15 min. During the event, the IMF and plasma parameters are highly perturbed producing several $P_{\rm dyn}$ peaks (Qpar jets) with values of up to 3 nPa. These values are much higher than ∼1 nPa in the ambient Qper plasma. The reason for the $P_{\rm dyn}$ peaks inside and at the rims of these flux tubes is beyond the scope of this paper. As mentioned before, the event is bounded by IMF rotations. We perform timing analysis of the event. In order to do so we found features that are recognizable in the data of all Cluster probes. We thus choose two short time intervals marked with vertical blue lines in Figure 3a. These intervals are exhibited in Figures 3b and 3c. We can see that the C3 spacecraft was the first to observe the event and was followed by C2, C4, and C1. Since this order of the spacecraft is the same during both time intervals, we conclude that this structure was also convected pass the Cluster probes and is again a flux tube connected to the Qpar bow-shock.

3.2. Nonreconnecting CS

Figure 4a features MMS1 observations during a 20-min time interval on November 16, 2015. The spacecraft GSE coordinates were (10.5, 0.02, −0.54) R_E. IMF and plasma parameters (in survey mode) indicate that during this time MMS1 was in the Qper magnetosheath except during 03:31:35–03:35:02 UT (shaded in purple), when a structure passed it. This event could be another flux tube albeit it is different from previous examples since it is less turbulent and the flux of ions with $E \lesssim 30$ keV in it is quite low. Alternatively, similar events were identified by Raptis, Karlsson, et al. (2020) as possible flux transfer events (Paschmann et al., 1982) due to enhanced B-field magnitude, depleted densities, increased temperature, the presence of ions with $E \lesssim 30$ keV, and the southward pointing IMF at the time of the events (see Petrinec et al., 2020). However, a bipolar IMF signature is missing in our case. Finally, this event is similar to reconnection jets due to magnetopause reconnection (Blanco-Cano et al., 2020), although these authors showed that such events exhibit ion distributions with two distinct populations, which is not the case here (Figure 4c iii). Hence, we will refer to this event simply as a "structure".

We now focus on a CS (Figure 4a, survey mode data) that produced a large $P_{\rm dyn}$ peak (∼1 nPa) at the upstream edge of the structure (vertical blue line). A short time interval exhibiting the CS in burst mode data is shown in Figure 4b. It is observed here that the $P_{\rm dyn}$ peaks at ∼2 nPa. There is an additional panel (x) that exhibits the electric current densities obtained by the curlometer method (black) and from particle moments (red). The CS exhibits some signatures reminiscent of REs, such as the drop of $B_{\rm tot}$, increases in ion density and velocity, and B-field and velocity rotations. In Figure 4d, which shows ion distributions before, during, and after the CS, we note that during the CS there are two populations present—one from the ambient magnetosheath and the second one with velocity >200 kms^{-1} parallel to the B-field. Although these ions might be accelerated in the CS itself, we note that ions with similar velocities in the plasma frame of reference also exist downstream of the CS, inside the "structure" (although there they appear at all angles with respect to the magnetic field) and could have simply leaked from there into the CS. Further evidence against this being a reconnecting CS is presented in Figure 4c. There we show the IMF magnitude (panel i), B-field components and velocity components (ii–vii) in the NLM coordinates. These were obtained by performing the minimum variance analysis (Sonnerup & Scheible, 1998) on the B-field data during the event. The velocity shown is a partial moment of the apparently accelerated component of the ion distribution function calculated for ion energies between ∼210 and 3,300 eV and pitch angles ≤45°. We can see that B and V components do not show the required correlations at one edge and anti-correlations at the other edge. Additionally, the Walén test (see Paschmann & Sonnerup, 2008, for details) in Figure 4e also suggest that this event is not a RE, since the changes in B and V do not exhibit the required (anti)correlations. Hence, we call this event a nonreconnecting CS.

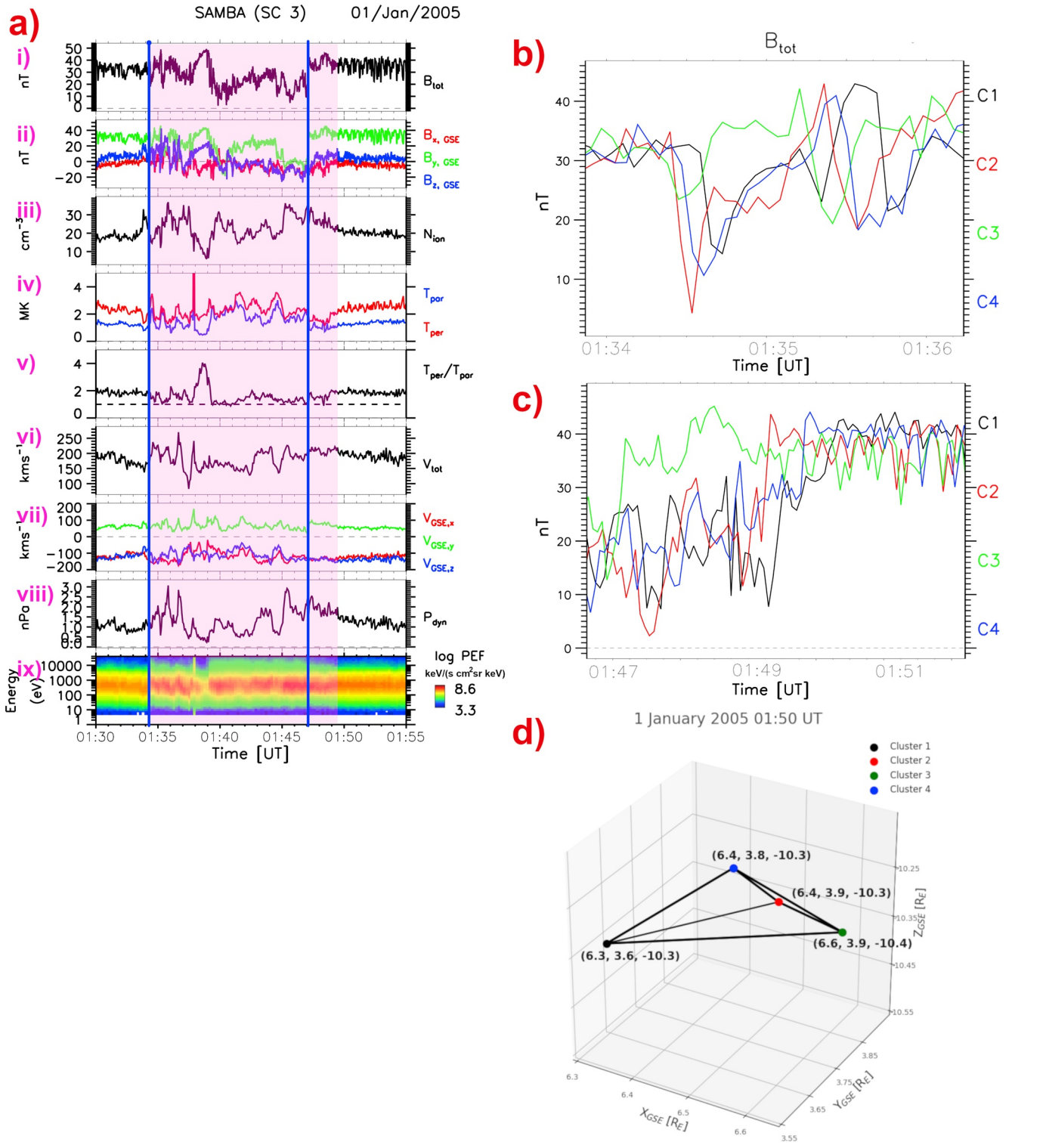

Figure 3. (a) Cluster-3 observations. The format is the same as in Figure 1a. (b and c) *B*-field profiles of the upstream and downstream edges of the flux tube in (left blue vertical lines in a) in all four Cluster spacecraft data. (d) Configuration of the Cluster constellation on January 1, 2005.

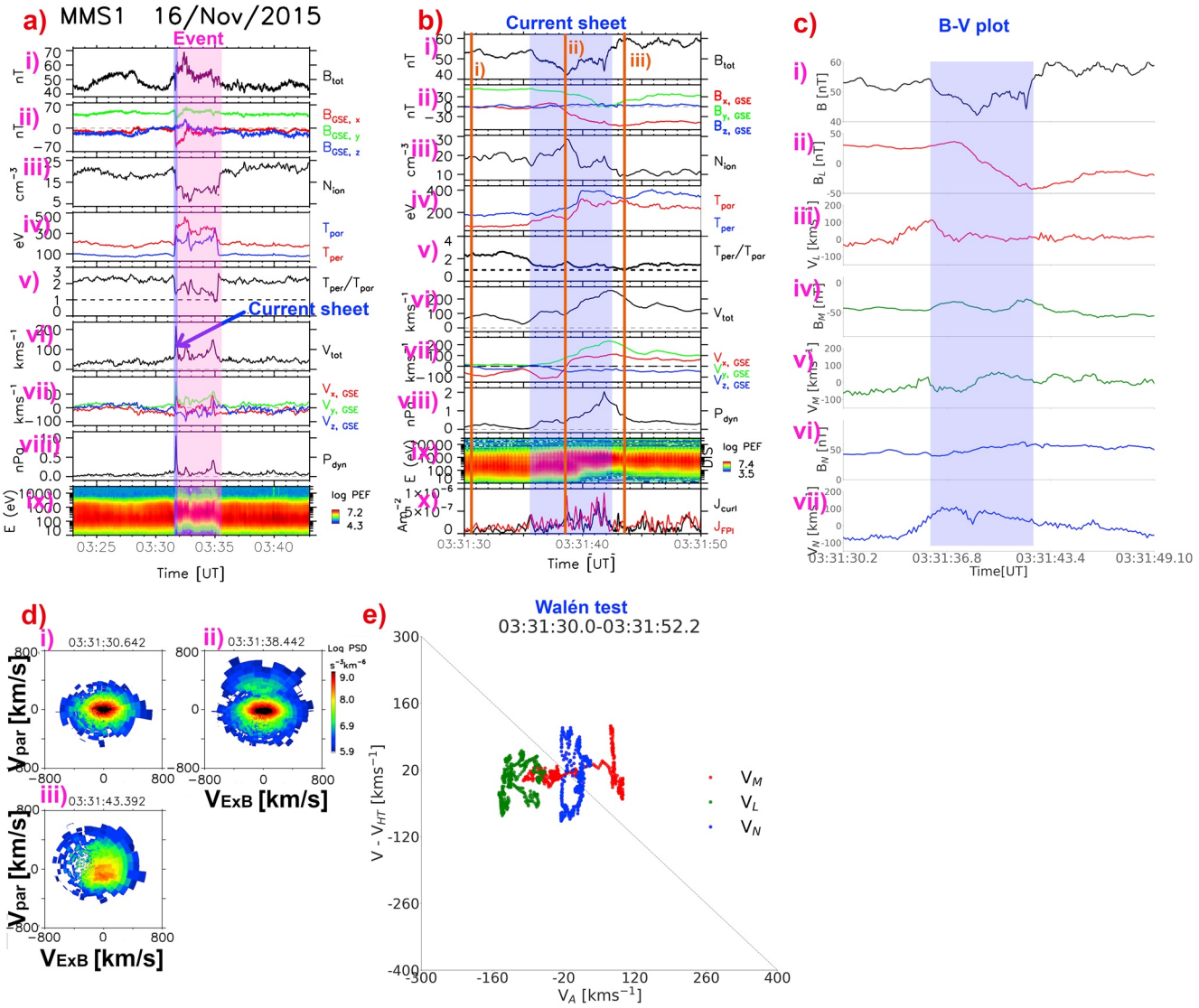

Figure 4. Magnetospheric Multiscale Mission (MMS) 1 observations of a nonreconnecting current sheet (CS) on November 16, 2015. (a) The event that caused the CS. (b) A detailed view of the CS. Vertical lines mark the times of ion distribution in Figure 4d. (b) *B-V* plot with (i) IMF magnitude, (ii–vii) IMF and velocity in the *N*, *L*, *M* coordinates. (d) Ion distributions before, during, and after the CS. On *x* (*y*) axis is the velocity perpendicular (parallel) to the *B*-field. (d) Walén test. On *y* axis is the ion velocity in the deHoffman-Teller frame and on *x* axis is the Alfvén velocity. The data are in the *LMN* coordinates (e.g., Vörös et al., 2017).

The higher bulk velocity in the spacecraft rest frame is thus mainly due to the acceleration of the primary magnetosheath ion population there. A possible explanation for the observed high velocity and P_{dyn} in the CS could be ion drifts caused by the magnetic field gradient and/or curvature across the CS.

3.3. Reconnection Exhaust

REs are ubiquitous in the pristine SW (e.g., Gosling et al., 2005). Although magnetic reconnection in the Qpar magnetosheath has been routinely observed by the MMS mission, ion jets originating from such regions, and thus REs, are not observed, except near the magnetopause. The lack of ion jets in the Qpar magnetosheath has been explained in terms of the high turbulence level present that does not permit their formation (e.g., Phan et al., 2018). The Qper magnetosheath is much less turbulent and REs have been observed there (e.g., Eastwood et al., 2018; Øieroset et al., 2017; Phan et al., 2007). Below we show an RE that produced large P_{dyn} values.

This event occurred on October 31, 2010 (Figure 5) due to a single IMF discontinuity. It was observed by the THEMIS-E spacecraft and was studied previously in a different context by Øieroset et al. (2017). At that time, THEMIS-E was located at (11.0, −11.6, 2.4) R_E in GSE coordinates. The IMF vectors before and after the exhaust in GSE coordinates were (−15.2, −25.8, −6.0) and (−1.9, −52.3, 20.5), respectively, meaning that the IMF rotated by ∼43° across the exhaust. The event lasted for ∼32 s in the data (shaded in purple). We can see on panel (viii) that this event produced a large P_{dyn} increase. P_{dyn} values before, during, and after the RE were 0.01, 0.23, and 0.1 nPa. Thus P_{dyn} inside the RE was increased by 2200% and 130% with respect to the upstream and downstream regions, respectively. Figure 5b shows *B*-field magnitude and GSE components of IMF and velocity. It can be observed that variations of *B* and *V* components are correlated on one side of the exhaust and anticorrelated on the other side, as it is expected for the REs.

3.4. Mirror Modes

MMs are ubiquitous in the magnetosheath (e.g., Dimmock et al., 2015). They exhibit compressive *B*-field fluctuations that are anticorrelated with the density and appear in the *B*-field data as dips or peaks. Magnetic dips are thus associated with density peaks and should produce P_{dyn} enhancements.

Here, we show MMS1 observations of MMs (Figure 5c) during a 10-min time interval on November 6, 2015, when the spacecraft were located at (11.0, 4.7, −0.8) R_E in GSE coordinates. An additional panel (x) features the so called mirror parameter $C_M = \beta_i \perp (\frac{T_i \perp}{T_i \parallel} - 1)$. This parameter was introduced by Génot et al. (2009). The values of $C_M > 1$ ($C_M < 1$) denote plasma that is, MM unstable (stable). We see that the plasma surrounding the MM waves is MM stable, while inside the MM waves it exhibits values of $C_M \gg 1$. Although the surrounding plasma is MM stable, it could have been unstable at earlier times when these waves were formed. Three most dominant MM waves are shaded in pink and marked as MM1, MM2, and MM3. These observations were made very near the magnetopause which was detected almost immediately after the featured time interval (not shown). In the *B*-field data, the three MMs appear as dips that represent between 72% and 93% decrease compared to ambient values. They exhibit density and temperature enhancements. The temperature anisotropy is slightly increased in the case of MM1, it does not stand out from the ambient values (∼1.8) for MM2 and is strongly, diminished in the case of MM3 (to ∼1.2, a 44% decrease).

The total velocity inside MM1 is not perturbed while it is increased inside MM2 (by ∼50%) and MM3 (by ∼116%) compared to their immediate neighborhood. The combination of density and velocity increases produces different signatures in the P_{dyn} data. Compared to their immediate neighborhood, the dynamic pressure inside these MMs is unchanged, increased by ∼270%, and increased by ∼250% inside MM1, MM2, and MM3, respectively. Due to the fact that the background P_{dyn} values are highest around MM3, this structure stands out on panel (viii). This event fulfills the observational criteria for a type of magnetosheath jets called diamagnetic plasmoids (Karlsson et al., 2012, 2015) due to the large density increase and *B*-field decrease.

4. Conclusions

In this work, we show that magnetosheath jets in the Qper magnetosheath may have a different origin than those in the Qpar magnetosheath. This is due to the fact that we do not expect to find magnetosheath jets produced at bow-shock ripples in the Qper magnetosheath.

We show that magnetosheath jet signatures can be produced by magnetic flux tubes that are embedded in the Qper magnetosheath but are connected to the Qpar section of the bow-shock. Inside them the IMF and plasma properties are the same as those typical of the Qpar magnetosheath, namely these quantities are more turbulent and the temperature anisotropy drops to ∼1. Either rims and/or the insides of the flux tubes may produce P_{dyn} peaks with values much higher than those in the surrounding Qper magnetosheath. We show that these flux tubes are convected pass the spacecraft by comparing their *B*-field profiles in the data of all Cluster probes. These flux tubes are the magnetosheath equivalent of foreshock cavities and traveling foreshocks commonly observed in the unperturbed upstream SW.

Next, we study a structure with a nonreconnecting CS at its upstream edge. This CS produced a magnetosheath jet with P_{dyn} of 2 nPa, which, compared to the ambient value of 0.5 nPa, represents an ∼3000%

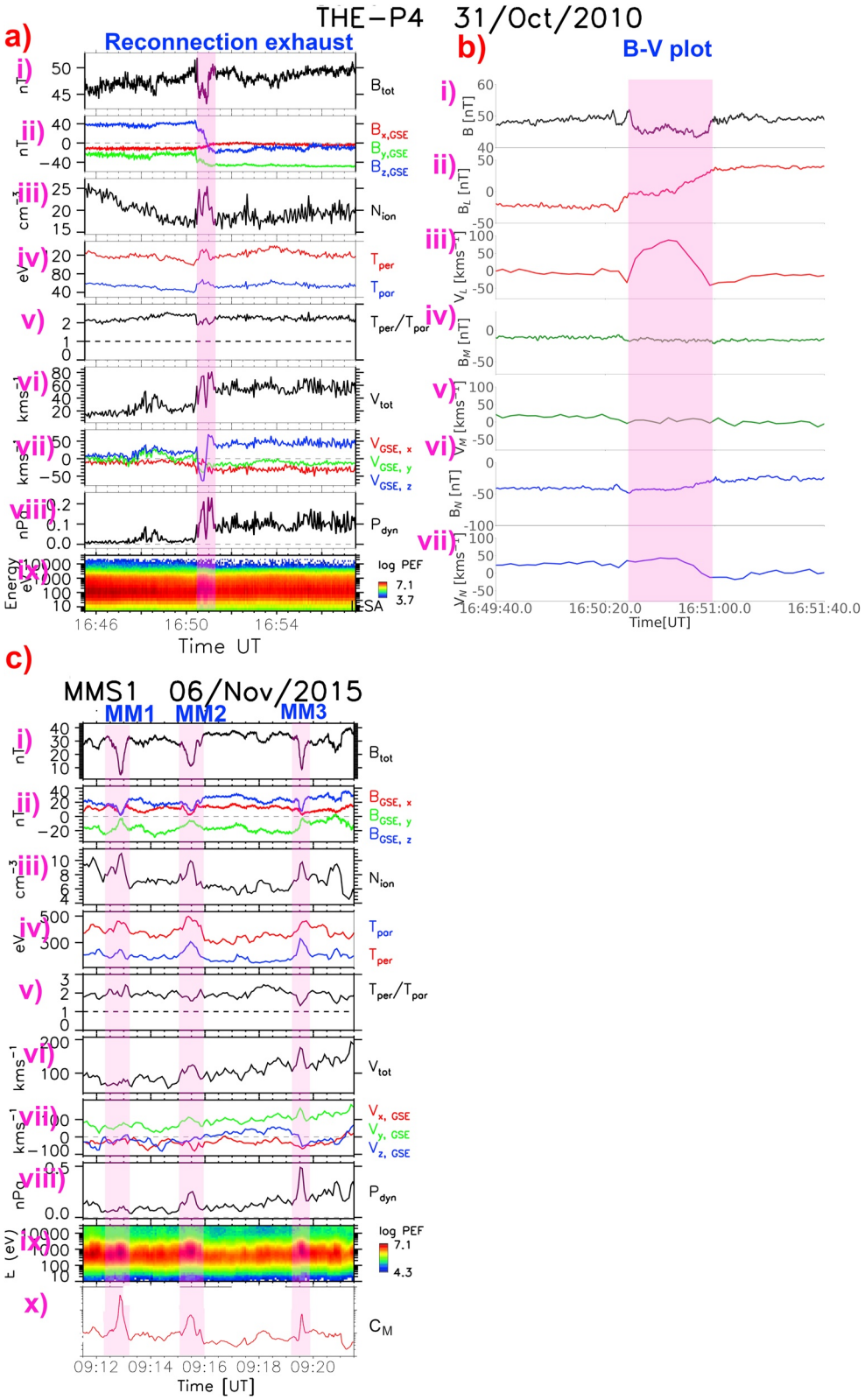

Figure 5. (a) THEMIS-E observations of a reconnection exhaust (shaded in purple) on October 31, 2010. The format of this figure is the same as that of Figure 2a. (b) *B-V* plot with (i) IMF magnitude, (ii–vii) IMF and velocity in the *N*, *L*, *M* coordinates, (c) Magnetospheric Multiscale Mission (MMS) 1 observations of mirror-mode (MM) waves (shaded) on November 6, 2015.

increase. We propose that the increased ion velocity and P_{dyn} in the CS may be due to the magnetic field gradient and/or curvature that produce ion drifts.

We further observe an RE in the Qper magnetosheath that occurred due to single IMF discontinuity and is thus similar to those observed in the pristine SW (e.g., Gosling et al., 2005). During this event, the P_{dyn} is increased by 1200% and 270% compared to ambient values before and after the event, respectively.

Finally, we show that MMs can also present important P_{dyn} enhancements. Two structures observed by MMS1 produced such peaks due to density and velocity enhancements inside them but only MM3 exhibited significant P_{dyn} increase due to the fact that it also exhibited total velocity increase.

One of the reasons for which it is important to study magnetosheath jets is that they may cause perturbations of the geomagnetic field even at the ground level (e.g., Archer & Horbury, 2013; Dmitriev & Suvorova, 2012). Magnetosheath jets of different origin occur during different interplanetary conditions. Associating their signatures with jet formation mechanisms will undoubtedly be a topic of future investigations.

Data Availability Statement

The original data sets are available at the Cluster Science Archive (SCA, https://www.cosmos.esa.int/web/csa) and the Coordinated Data Analysis Web (CDAWeb, https://cdaweb.gsfc.nasa.gov/).

Acknowledgments
The authors acknowledge the ClWeb team (http://clweb.irap.omp.eu/) for easy access to the data. Most of the figures were produced with ClWeb. Primož Kajdič's work was supported by the UNAM DGAPA/PAPIIT grant IN-105620. Savvas Raptis and Tomas Karlsson were supported by the Swedish National Space Agency (SNSA grant 90/17). Xóchitl Blanco-Cano's work was supported by the UNAM DGAPA PAPIIT IN-110921 grant.

References

Angelopoulos, V. (2008). The THEMIS mission. *Space Science Reviews*, *141*(1–4), 5–34. https://doi.org/10.1007/s11214-008-9336-1

Archer, M. O., & Horbury, T. S. (2013). Magnetosheath dynamic pressure enhancements: Occurrence and typical properties. *Annales Geophysicae*, *31*, 319–331. https://doi.org/10.5194/angeo-31-319-2013

Archer, M. O., Horbury, T. S., & Eastwood, J. P. (2012). Magnetosheath pressure pulses: Generation downstream of the bow shock from solar wind discontinuities. *Journal of Geophysical Research*, *117*, A05228. https://doi.org/10.1029/2011JA017468

Auster, H. U., Glassmeier, K. H., Magnes, W., Aydogar, O., Baumjohann, W., Constantinescu, D., et al. (2008). The THEMIS fluxgate magnetometer. *Space Science Reviews*, *141*(1–4), 235–264. https://doi.org/10.1007/s11214-008-9365-9

Balogh, A., Carr, C. M., Acuña, M. H., Dunlop, M. W., Beek, T. J., Brown, P., et al. (2001). The cluster magnetic field investigation: Overview of in-flight performance and initial results. *Annales Geophysicae*, *19*(10/12), 1207–1217. https://doi.org/10.5194/angeo-19-1207-2001

Billingham, L., Schwartz, S. J., & Sibeck, D. G. (2008). The statistics of foreshock cavities: Results of a Cluster survey. *Annales Geophysicae*, *26*, 3653–3667. https://doi.org/10.5194/angeo-26-3653-2008

Blanco-Cano, X., Preisser, L., Kajdič, P., & Rojas-Castillo, D. (2020). Magnetosheath microstructure: Mirror mode waves and jets during southward IP magnetic field. *Journal of Geophysical Research: Space Physics*, *125*(9), e27940. https://doi.org/10.1029/2020JA027940

Burgess, D. (1989). Cyclic behavior at quasi-parallel collisionless shocks. *Geophysical Research Letters*, *16*(5), 345–348. https://doi.org/10.1029/GL016i005p00345

Dimmock, A. P., Osmane, A., Pulkkinen, T. I., & Nykyri, K. (2015). A statistical study of the dawn-dusk asymmetry of ion temperature anisotropy and mirror mode occurrence in the terrestrial dayside magnetosheath using THEMIS data. *Journal of Geophysical Research: Space Physics*, *120*(7), 5489–5503. https://doi.org/10.1002/2015JA021192

Dmitriev, A. V., & Suvorova, A. V. (2012). Traveling magnetopause distortion related to a large-scale magnetosheath plasma jet: THEMIS and ground-based observations. *Journal of Geophysical Research*, *117*, A08217. https://doi.org/10.1029/2011JA016861

Eastwood, J. P., Balogh, A., Lucek, E. A., Mazelle, C., & Dandouras, I. (2005). Quasi-monochromatic ulf foreshock waves as observed by the four-spacecraft cluster mission: 1. statistical properties. *Journal of Geophysical Research*, *110*(A11), A11219. https://doi.org/10.1029/2004JA010617

Eastwood, J. P., Mistry, R., Phan, T. D., Schwartz, S. J., Ergun, R. E., Drake, J. F., et al. (2018). Guide Field reconnection: Exhaust structure and heating. *Geophysical Research Letters*, *45*(10), 4569–4577. https://doi.org/10.1029/2018GL077670

Escoubet, C., Schmidt, R., & Goldstein, M. (1997). Cluster—Science and mission overview. *Space Science Reviews*, *79*(1), 11–32. https://doi.org/10.1023/A:1004923124586

Génot, V., Budnik, E., Hellinger, P., Passot, T., Belmont, G., Trávníček, P. M., et al. (2009). Mirror structures above and below the linear instability threshold: Cluster observations, fluid model and hybrid simulations. *Annales Geophysicae*, *27*(2), 601–615. https://doi.org/10.5194/angeo-27-601-2009

Giacalone, J., Schwartz, S. J., & Burgess, D. (1993). Observations of suprathermal ions in association with slams. *Geophysical Research Letters*, *20*(2), 149–152. https://doi.org/10.1029/93GL00067

Gosling, J. T., Eriksson, S., McComas, D. J., Skoug, R. M., & Forsyth, R. J. (2005). Reconnection exhausts in the solar wind well beyond 1 AU: Ulysses (2005, p. SM13C-04). Agu fall meeting abstracts.

Gutynska, O., Sibeck, D. G., & Omidi, N. (2015). Magnetosheath plasma structures and their relation to foreshock processes. *Journal of Geophysical Research: Space Physics*, *120*, 7687–7697. https://doi.org/10.1002/2014JA020880

Hietala, H., Phan, T. D., Angelopoulos, V., Oieroset, M., Archer, M. O., Karlsson, T., & Plaschke, F. (2018). In situ observations of a magnetosheath high-speed jet triggering magnetopause reconnection. *Geophysical Research Letters*, *45*(4), 1732–1740. https://doi.org/10.1002/2017GL076525

Hietala, H., & Plaschke, F. (2013). On the generation of magnetosheath high-speed jets by bow shock ripples. *Journal of Geophysical Research: Space Physics*, *118*, 7237–7245. https://doi.org/10.1002/2013JA019172

Hietala, N., Laitinen, T. V., Clausen, L. B. N., Facskó, G., Vaivads, A., Koskinen, H. E. J., et al. (2012). Supermagnetosonic subsolar magnetosheath jets and their effects: From the solar wind to the ionospheric convection. *Annales Geophysicae*, *30*, 33–48. https://doi.org/10.5194/angeo-30-33-2012

Hietala, T. V., Andréeová, K., Vainio, R., Vaivads, A., Palmroth, M., Pulkkinen, T., et al. (2009). Supermagnetosonic jets behind a collisionless quasiparallel shock. *Physical Review Letters*, *103*(24), 245001. https://doi.org/10.1103/PhysRevLett.103.245001

Kajdič, P., Blanco-Cano, X., Omidi, N., Rojas-Castillo, D., Sibeck, D. G., & Billingham, L. (2017). Traveling foreshocks and transient foreshock phenomena. *Journal of Geophysical Research: Space Physics*, *122*(9), 9148–9168. https://doi.org/10.1002/2017JA023901

Karlsson, T., Brenning, N., Nilsson, H., Trotignon, J.-G., Vallières, X., & Facsko, G. (2012). Localized density enhancements in the magnetosheath: Three-dimensional morphology and possible importance for impulsive penetration. *Journal of Geophysical Research*, *117*, A03227. https://doi.org/10.1029/2011JA017059

Karlsson, T., Kullen, A., Liljeblad, E., Brenning, N., Nilsson, H., Gunell, H., & Hamrin, M. (2015). On the origin of magnetosheath plasmoids and their relation to magnetosheath jets. *Journal of Geophysical Research: Space Physics*, *120*, 7390–7403. https://doi.org/10.1002/2015JA021487

Katrcolu, F. T., Kaymaz, Z., Sibeck, D. G., & Dandouras, I. (2009). Magnetosheath cavities: Case studies using cluster observations. *Annales Geophysicae*, *27*(10), 3765–3780. https://doi.org/10.5194/angeo-27-3765-2009

Krauss-Varban, D., & Omidi, N. (1991). Structure of medium Mach number quasi-parallel shocks: Upstream and downstream waves. *Journal of Geophysical Research*, *96*(A10), 17715–17731. https://doi.org/10.1029/91JA0154510.1029/91JA01545

Liu, T. Z., Hietala, H., Angelopoulos, V., Omelchenko, Y., Vainio, R., & Plaschke, F. (2020). Statistical study of magnetosheath jet-driven bow waves. *Journal of Geophysical Research: Space Physics*, *125*(7), e2019JA027710. https://doi.org/10.1029/2019JA027710

Lucek, E. A., Constantinescu, D., Goldstein, M. L., Pickett, J., Pinçon, J. L., Sahraoui, F., et al. (2005). The magnetosheath. *Space Science Reviews*, *118*(1–4), 95–152. https://doi.org/10.1007/s11214-005-3825-2

Lucek, E. A., Horbury, T. S., Balogh, A., Dandouras, I., & Rème, H. (2004). Cluster observations of hot flow anomalies. *Journal of Geophysical Research*, *109*, A06207. https://doi.org/10.1029/2003JA010016

McFadden, J. P., Carlson, C. W., Larson, D., Ludlam, M., Abiad, R., Elliott, B., et al. (2008). The THEMIS ESA plasma instrument and in-flight calibration. *Space Science Reviews*, *141*(1–4), 277–302. https://doi.org/10.1007/s11214-008-9440-2

Øieroset, M., Phan, T. D., Shay, M. A., Haggerty, C. C., Fujimoto, M., Angelopoulos, V., et al. (2017). THEMIS multispacecraft observations of a reconnecting magnetosheath current sheet with symmetric boundary conditions and a large guide field. *Geophysical Research Letters*, *44*(15), 7598–7606. https://doi.org/10.1002/2017GL074196

Omidi, N., Sibeck, D., Blanco-Cano, X., Rojas-Castillo, D., Turner, D., Zhang, H., & Kajdič, P. (2013). Dynamics of the foreshock compressional boundary and its connection to foreshock cavities. *Journal of Geophysical Research: Space Physics*, *118*, 823–831. https://doi.org/10.1002/jgra.50146

Paschmann, G., Haerendel, G., Papamastorakis, I., Sckopke, N., Bame, S. J., Gosling, J. T., & Russell, C. T. (1982). Plasma and magnetic field characteristics of magnetic flux transfer events. *Journal of Geophysical Research*, *87*(A4), 2159–2168. https://doi.org/10.1029/JA087iA04p02159

Paschmann, G., & Sonnerup, B. U. O. (2008). Proper frame determination and Walen test. In G. Paschmann & P. W. Daly (Eds.), *Multi-spacecraft analysis methods revisited* (ISSI Scientific Reports Series 8, pp. 65–74).

Petrinec, S. M., Burch, J. L., Chandler, M., Farrugia, C. J., Fuselier, S. A., Giles, B. L., et al. (2020). Characteristics of minor ions and electrons in flux transfer events observed by the Magnetospheric Multiscale Mission. *Journal of Geophysical Research: Space Physics*, *125*(7), e27778. https://doi.org/10.1029/2020JA027778

Phan, T. D., Eastwood, J. P., Shay, M. A., Drake, J. F., Sonnerup, B. U. Ö., Fujimoto, M., et al. (2018). Electron magnetic reconnection without ion coupling in Earth's turbulent magnetosheath. *Nature*, *557*(7704), 202–206. https://doi.org/10.1038/s41586-018-0091-5

Phan, T. D., Paschmann, G., Twitty, C., Mozer, F. S., Gosling, J. T., Eastwood, J. P., et al. (2007). Evidence for magnetic reconnection initiated in the magnetosheath. *Geophysical Research Letters*, *34*, L14104. https://doi.org/10.1029/2007GL030343

Plaschke, F., & Glassmeier, K.-H. (2011). Properties of standing Kruskal-Schwarzschild-modes at the magnetopause. *Annales Geophysicae*, *29*, 1793–1807. https://doi.org/10.5194/angeo-29-1793-2011

Plaschke, F., Hietala, H., & Angelopoulos, V. (2013). Anti-sunward high-speed jets in the subsolar magnetosheath. *Annales Geophysicae*, *31*, 1877–1889. https://doi.org/10.5194/angeo-31-1877-2013

Plaschke, F., Hietala, H., Angelopoulos, V., & Nakamura, R. (2016). Geoeffective jets impacting the magnetopause are very common. *Journal of Geophysical Research: Space Physics*, *121*, 3240–3253. https://doi.org/10.1002/2016JA022534

Plaschke, F., Hietala, M., Blanco-Cano, X., Kajdič, P., Karlsson, T., Lee, S. H., et al. (2018). Jets downstream of collisionless shocks. *Space Science Reviews*, *214*(5), 81. https://doi.org/10.1007/s11214-018-0516-3

Pollock, C., Moore, T., Jacques, A., Burch, J., Gliese, U., Saito, Y., et al. (2016). Fast plasma investigation for magnetospheric multiscale. *Space Science Reviews*, *199*(1), 331–406. https://doi.org/10.1007/s11214-016-0245-4

Raptis, S., Aminalragia-Giamini, S., Karlsson, T., & Lindberg, M. (2020). Classification of magnetosheath jets using neural networks and high resolution OMNI (HRO) data. *Frontiers in Astronomy and Space Sciences*, *7*, 24. https://doi.org/10.3389/fspas.2020.00024

Raptis, S., Karlsson, T., Plaschke, F., Kullen, A., & Lindqvist, P.-A. (2020). Classifying magnetosheath jets using mms: Statistical properties. *Journal of Geophysical Research: Space Physics*, *125*(11), e2019JA027754. https://doi.org/10.1029/2019JA027754

Rème, H., Aoustin, C., Bosqued, J. M., Dandouras, I., Lavraud, B., Sauvaud, J. A., et al. (2001). First multispacecraft ion measurements in and near the Earth's magnetosphere with the identical Cluster ion spectrometry (CIS) experiment. *Annales Geophysicae*, *19*, 1303–1354. https://doi.org/10.5194/angeo-19-1303-2001

Russell, C. T., Anderson, B. J., Baumjohann, W., Bromund, K. R., Dearborn, D., Fischer, D., et al. (2016). The magnetospheric multiscale magnetometers. *Space Science Reviews*, *199*(1), 189–256. https://doi.org/10.1007/s11214-014-0057-3

Savin, S., Amata, E., Zelenyi, L., Nemecek, Z., Borodkova, N., Buechner, J., et al. (2012). Super fast plasma streams as drivers of transient and anomalous magnetospheric dynamics. *Annales Geophysicae*, *30*, 1–7. https://doi.org/10.5194/angeo-30-1-2012

Sharma, A. S., & Curtis, S. A. (2005). Magnetospheric multiscale mission, In *Nonequilibrium phenomena in plasmas* (pp. 179–195). Springer Netherlands. https://doi.org/10.1007/1-4020-3109-2_8

Shue, J.-H., Chao, J.-K., Song, P., McFadden, J. P., Suvorova, A., Angelopoulos, V., et al. (2009). Anomalous magnetosheath flows and distorted subsolar magnetopause for radial interplanetary magnetic fields. *Geophysical Research Letters*, *36*, L18112. https://doi.org/10.1029/2009GL039842

Sibeck, D. G., Kudela, K., Lepping, R. P., Lin, R., Nemecek, Z., Nozdrachev, M. N., et al. (2000). Magnetopause motion driven by interplanetary magnetic field variations. *Journal of Geophysical Research*, *105*, 25155–25169. https://doi.org/10.1029/2000JA900109

Sibeck, D. G., Phan, T.-D., Lin, R., Lepping, R. P., & Szabo, A. (2002). Wind observations of foreshock cavities: A case study. *Journal of Geophysical Research*, *107*, 1271. https://doi.org/10.1029/2001JA007539

Sonnerup, B. U. Ö., & Scheible, M. (1998). Minimum and maximum variance analysis. In G. Paschmann, & P. Daly (Eds.), *Analysis methods for multi-spacecraft data* (pp. 185–220). ESA. Retrieved from http://adsabs.harvard.edu/abs/1998ISSIR\ldots1\enleadertwodots185S

Treumann, R. A. (2009). Fundamentals of collisionless shocks for astrophysical application, 1. Non-relativistic shocks. *Astronomy and Astrophysics Review*, *17*(4), 409–535. https://doi.org/10.1007/s00159-009-0024-2

Tsurutani, B. T., & Stone, R. G. (1985). Collisionless shocks in the heliosphere: Reviews of current research (Geophysical Monograph Series, 35). American Geophysical Union. https://doi.org/10.1029/GM035

Vörös, Z., Yordanova, E., Varsani, A., Genestreti, K. J., Khotyaintsev, Y. V., Li, W., et al. (2017). MMS observation of magnetic reconnection in the turbulent magnetosheath. *Journal of Geophysical Research: Space Physics*, *122*(11), 11442–11467. https://doi.org/10.1002/2017JA024535

Wang, B., Nishimura, Y., Hietala, H., Lyons, L., Angelopoulos, V., Plaschke, F., et al. (2018). Impacts of magnetosheath high-speed jets on the magnetosphere and ionosphere measured by optical imaging and satellite observations. *Journal of Geophysical Research: Space Physics*, *123*(6), 4879–4894. https://doi.org/10.1029/2017ja024954